Surfaces and Interfaces 46 (2024) 103780

Contents lists available at ScienceDirect

Surfaces and Interfaces

journal homepage: www.sciencedirect.com/journal/surfaces-and-interfaces

Phase control of heterogeneous 1T/2H-MoS_2 to improve the selective catalytic reduction activity of VMo/Ti

Su-Jin Kim [a,b], Donghyeok Kim [a,b], Myeung-Jin Lee [a,b], Woon-Gi Kim [a,c], Bora Jeong [a,c], Bora Ye [a,*], Hong-Dae Kim [a,*]

[a] Green Materials & Processes R&D Group, Korea Institute of Industrial Technology, Ulsan, 44413, Republic of Korea
[b] Department of Materials Science and Engineering, Ulsan National Institute of Science and Technology, Ulsan 44919, Republic of Korea
[c] Department of Material Science and Engineering, Pusan National University, Busan 46241, Republic of Korea

ARTICLE INFO

Keywords:
1T/2H-MoS_2
Phase control
2D materials
NH_3-SCR catalyst
VMo/TiO_2 catalyst

ABSTRACT

V_2O_5-WO_3(MoO_3)/TiO_2 catalysts have been widely used for NO_X removal owing to their excellent catalytic performance; however, they suffer from a narrow operating temperature range, reduced N_2 selectivity at a high temperature, and deteriorated activity due to SO_2 poisoning. In this study, a phase-controlled 1T/2H-MoS_2 was prepared by a one-step hydrothermal method and used as a Mo precursor to develop V-Mo/Ti catalysts with improved selective catalytic reduction (SCR) performance. Raman analysis confirmed that the heterogeneous MoS_2 contains a partially formed 1T phase, which facilitated the generation of active sites in the catalyst. The heterogeneous 1T/2H-MoS_2 also produced a considerable amount of surface oxygen species on the V-Mo/Ti catalyst, which increased the $V^{4+}/(V^{4+}+V^{5+})$ ratio. The resulting catalyst maintained a NO_X conversion of over 96% from 250°C to 400°C and demonstrated excellent N_2 selectivity and resistance to SO_2 poisoning.

1. Introduction

Nitrogen oxides (NO_X), such as NO and NO_2, are the oxidation products of nitrogen in fuels during combustion. They are emitted by thermal power plants, industrial boilers, incinerators, steel mills, ships, etc. [1,2,3] As the major source of acid rain, NO_X can cause severe air pollution, including generating secondary pollutants (ozone and peroxyacetyl nitrate) via photochemical reactions that are toxic and harmful to human health [4,5]. Environmental regulations have set more stringent emission standards for various industrial facilities, including ships and cement kilns. Consequently, post-treatment of nitrogen oxides is an important research topic and highly desirable for the protection and preservation of the environment [6,7,8,9].

The NH_3-selective catalytic reduction (NH_3-SCR) system is one of the most promising technologies to convert NO_X into harmless products [10,11]. SCR catalysts are composed of various transition metal oxides. Among them, V_2O_5-WO_3(MoO_3)/TiO_2 catalysts are widely used for NO_X removal owing to their excellent catalytic activity and N_2 selectivity [12,13]. However, vanadium-based catalysts have a narrow operating temperature range between 300–350°C, and their N_2 selectivity decreases at relatively high temperatures [14,15]. The stationary source SCR system in the power plants, steel mills, and industrial boilers may encounter exhaust gas with lower temperatures than the optimal operating temperature of the catalyst during start-up, shutdown, and low-load operation. Furthermore, for the system in power plant, the dust-containing exhaust gas passes through an electrostatic precipitator (ESP) before additional heat is supplied to activate the V-based catalysts. Therefore, it is essential to achieve high NO_X conversion efficiency and excellent N_2 selectivity over a wide temperature range from 250 to 400°C. Another critical challenge in NH_3-SCR technology is that the presence of SO_2 in the exhaust gas can form toxic vanadium species and deactivate the catalyst [16,17,18].

Molybdenum disulfide (MoS_2) has been extensively investigated owing to its two-dimensional layered structure and high catalytic activity [19,20]. MoS_2 exists as a thermodynamically stable 2H (hexagonal) phase and possesses semiconductor properties, but its active sites exist only at the edges, and the basic plane is chemically inactive [21]. In contrast, metallic 1T (trigonal) phase MoS_2 demonstrates enhanced catalytic activity owing to abundant active sites on its surface and high electrical conductivity [20,22,23].

In this study, to improve the SCR catalytic performance of vanadium-based catalysts, heterogeneous 1T/2H-MoS_2 was synthesized via an in-

* Corresponding author.
E-mail address: hdkim@kitech.re.kr (H.-D. Kim).

https://doi.org/10.1016/j.surfin.2023.103780
Received 11 September 2023; Received in revised form 13 December 2023; Accepted 16 December 2023
Available online 23 December 2023

situ one-step hydrothermal process in the presence of a moderate amount of propionic acid [24]. Subsequently, the VMo/Ti catalysts were prepared using an impregnation method for the NH_3-SCR reaction, and the catalytic activity of the synthesized catalysts was evaluated for NH_3-SCR, and their SO_2 resistance was measured under harsh conditions involving 300 ppm SO_2 and a gas hourly space velocity (GHSV) of 120,000 h^{-1}. The heterogeneous 1T/2H-MoS_2 demonstrated excellent N_2 selectivity by forming a considerable amount of surface oxygen species on the V-Mo/Ti catalyst. The higher $V^{4+}/(V^{4+}+V^{5+})$ ratio enhanced the NO_X conversion in a wide temperature range of 250–400°C. Additionally, the $Mo^{6+}/(Mo^{5+}+Mo^{6+})$ ratio was increased due to the addition of MoS_2, which effectively prevented the catalyst from SO_2 poisoning.

2. Experimental

2.1. Synthesis of heterogeneous 1T/2H-MoS_2

Heterogeneous 1T/2H-MoS_2 was prepared using a one-step hydrothermal method [22,25,26,27]. In a typical procedure, sodium molybdate dehydrate ($Na_2MoO_4{\cdot}2H_2O$) (99.5% Sigma Aldrich) and thiourea ($CS(NH_2)_2$) (99% Sigma Aldrich) in a specified ratio were dissolved in a mixed solvent (48 mL of deionized water and 24 mL of propionic acid). The mixture was stirred vigorously for 30 min and subsequently transferred into a 100 mL Teflon-lined steel autoclave, followed by heat treatment in a drying oven at 180°C for 4 h. The autoclave was rapidly cooled to room temperature. The 1T/2H-MoS_2 powder was collected via vacuum-assisted filtration, washed three times with distilled water by centrifugation, and dried overnight in an air oven.

2.2. Catalyst preparation

In this study, vanadium-based catalysts were synthesized using a wet impregnation method. Titanium dioxide powder (>97%, NANO Co., Ltd.) was used as a support for all the catalysts [28,29]. Ammonium metavanadate (NH_4VO_3) (99% Sigma Aldrich) was dissolved in 50 mL of ethanol (EtOH) solution, and an appropriate amount of diluted citric acid was added to adjust the pH [30,31]. Different Mo precursors, i.e., ammonium molybdate tetrahydrate ($(NH_4)_6Mo_7O_{24}{\cdot}4H_2O$) (99%, Daejung Chemicals), the synthesized 1T/2H-MoS_2, and 2H-MoS_2 (crystal, 99%, Sigma Aldrich), were individually stirred in 100 mL of EtOH for 1 h to form three separate dispersions. Then, 4.65 g of TiO_2 was dispersed in EtOH (100 mL) and mixed with the above dispersion. The mixture was evaporated in an oil bath at 70°C. The obtained powder was subsequently calcined in air at 500°C for 4 h. The catalysts synthesized using different Mo precursors were denoted as VMo/Ti, $VMoS_2$(H)/Ti, and $VMoS_2$(T)/Ti.

2.3. Measurement of catalytic performance

The SCR performance of the catalysts was evaluated in a fixed-bed reactor containing a quartz tube reactor with an inner diameter of 8 mm. The evolution gas mixture consisted of 300 ppm NH_3, 300 ppm NO_X, 5 vol% O_2, and N_2 balance gas. For each test, 0.5 mL of catalyst was charged, and the temperature was increased from 150 to 400°C in 50°C increments with a GHSV of 120,000 h^{-1}. All the reaction gases were injected into the reactor using a mass flow controller (MKS Co.), mixed, and passed through the catalysts in the reactor. The SO_2-poisoning test was conducted at 200°C for 6 h using the same gas conditions as mentioned above with an additional 300 ppm of SO_2. The SCR performance of the NO_X conversion and N_2 selectivity were calculated using the following equations.

$$NO_x\ conversion(\%) = \frac{[NO_x]_{in} - [NO]_{out} - [NO_2]_{out}}{[NO_x]_{in}} \times 100\% \quad (1)$$

$$N_2\ selectivity(\%) = \frac{[NO]_{in} - [NO]_{out} + [NH_3]_{in} - [NH_3]_{out} + [NO_2]_{out} - 2[N_2O]_{out}}{[NO]_{in} - [NO]_{out} + [NH_3]_{in} - [NH_3]_{out}} \times 100\% \quad (2)$$

2.4. Characterization of the catalysts

Field-emission scanning electron microscopy (FE-SEM, Hitachi, SU800) was used to characterize the morphology of MoS_2 at 20 kV

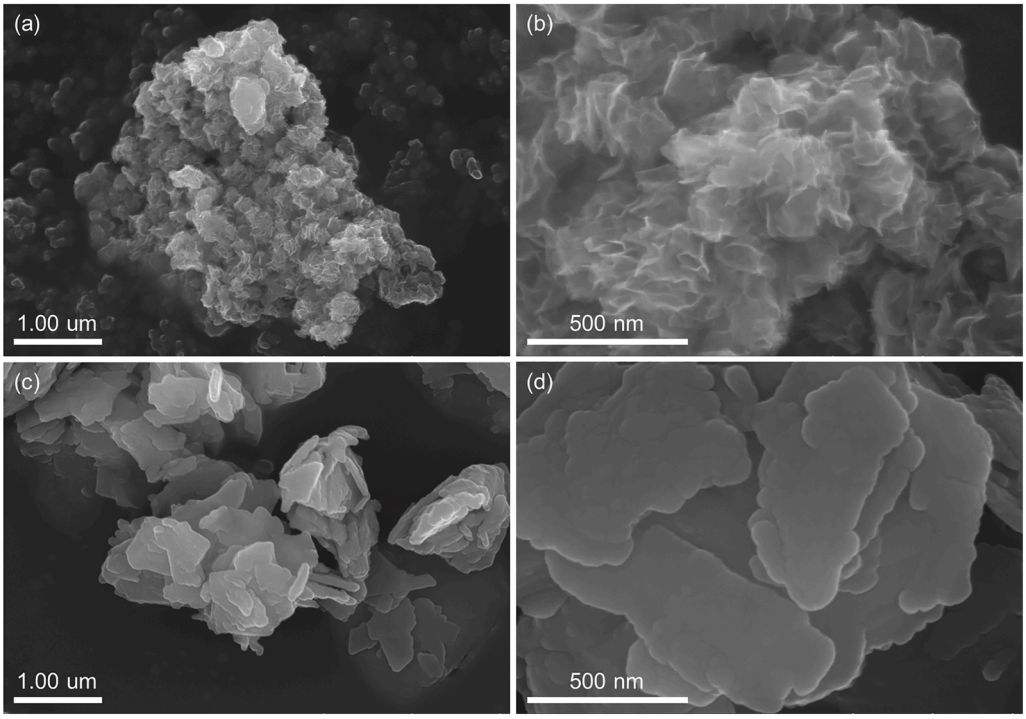

Fig. 1. SEM images of (a,b) 1T/2H-MoS_2 and (c,d) bulk 2H-MoS_2.

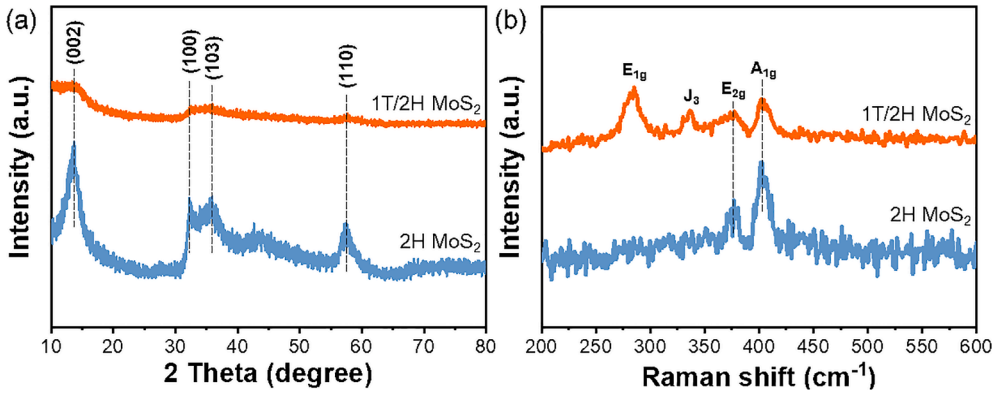

Fig. 2. (a) XRD patterns and (b) Raman spectra of 1T/2H-MoS_2 and 2H-MoS_2.

Table 1
BET characterization results of VMo/Ti, $VMoS_2$(H)/Ti, and $VMoS_2$(T)/Ti catalysts.

Sample	Specific surface area (m^2g^{-1})	Pore volume (cm^3g^{-1})	Average pore size (nm)
VMo/Ti	77	0.32	16.3
$VMoS_2$(H)/Ti	72	0.31	17.2
$VMoS_2$(T)/Ti	77	0.32	16.9

acceleration voltage. X-ray diffraction (XRD, Bruker, D8 Advanced) was performed with a Cu Kα radiation source (λ = 0.15406 nm) over the 2θ range of 10–80° (per 0.02°) at a scan speed of 4°/min. Raman spectra were obtained to confirm the MoS_2 phase states using a confocal Raman spectrometer (WITec, Alpha 300R) with a laser wavelength of 532 nm at 0.2 mW. The pore characteristics of each sample were determined using N_2 adsorption-desorption equipment (Micrometrics, ASAP 2020). The specific surface area was measured using the Brunauer-Emmett-Teller (BET) equation, and the pore size and diameter were obtained using the Barrett-Joyner-Halenda (BJH) method. Approximately 0.2–0.3 g of the samples were pretreated in a vacuum at 150°C for 4 h to remove adsorbed water and impurities. X-ray photoelectron spectroscopy (XPS, Thermo Fisher Scientific, NexsaG2 Surface Analysis System) was performed using an Al Kα radiation source (λ = 0.154 06 nm) to obtain the valence state of each element. FTIR spectroscopy (FT-IR, Bruker, Vertex 80v) was performed to analyze the functional groups on the surface after poisoning with various catalysts to confirm the effect of MoS_2 on SO_2-resistance enhancement.

3. Results and discussion

3.1. Morphological and structural analysis of 1T/2H-MoS_2 and 2H-MoS_2

To confirm that the heterogeneous 1T/2H-MoS_2 was successfully synthesized, its morphology was examined using SEM. The images in Fig. 1 (a and b) show that the 1T/2H-MoS_2 synthesized via the one-step hydrothermal method contains flower-like nanoparticles. Although some agglomeration is observed, the particle size of 1T/2H-MoS_2 is smaller than that of bulk 2H-MoS_2. This can be attributed to the insufficient crystal growth of MoS_2 within a relatively short synthesis time owing to the formation of 1T phase-MoS_2 in the initial reaction [27]. In contrast, Fig. 1(c and d) show the SEM images of bulk-MoS_2, revealing a relatively large irregular overlapped plate-like structure.

SEM images cannot prove that the directly manufactured MoS_2 is a heterogeneous mixture of 1T and 2H phases; therefore, additional characterizations were performed using XRD and Raman spectroscopy [27,32]. The XRD patterns of 1T/2H-MoS_2 and bulk MoS_2 (Fig. 2a) reveal the characteristic peaks of 2H-MoS_2 in both cases. The broad XRD peak with a low intensity in 1T/2H-MoS_2 suggests its sufficiently small crystalline size [33,24,34]. The Raman spectra of 1T/2H-MoS_2 and 2H-MoS_2 (Fig. 2b) show the main characteristic peaks of 2H-MoS_2 at E_{2g} (376 cm^{-1}) and A_{1g} (401 cm^{-1}) modes, consistent with the XRD results [25,35]. In addition, the Raman spectrum of 1T/2H-MoS_2 exhibits E_{1g} (285cm^{-1}) and J_3 (336cm^{-1}) modes of 1T phase, demonstrating that the heterogeneous 1T/2H-MoS_2 with a partial 1T phase along with the 2H phase was successfully synthesized through the reduction-first hypothesis theory using propionic acid [25,36].

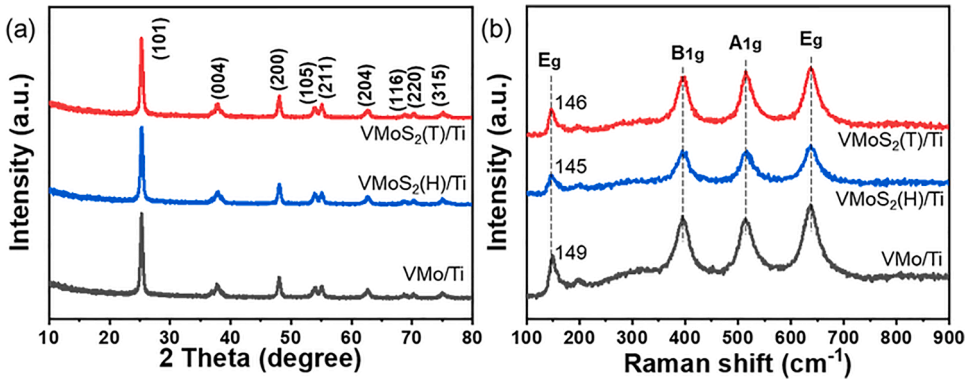

Fig. 3. (a) XRD patterns and (b) Raman spectra of VMo/Ti, $VMoS_2$(H)/Ti, and $VMoS_2$(T)/Ti catalysts.

Table 2
XRF results of VMo/Ti, $VMoS_2$(H)/Ti, and $VMoS_2$(T)/Ti catalysts

Catalysts	V_2O_5 (%)	MoO_3 (%)	TiO_2 (%)	SO_3 (%)
VMo/Ti	1.88	5.96	87.49	0.34
$VMoS_2$(H)/Ti	1.86	4.67	87.19	3.50
$VMoS_2$(T)/Ti	1.87	4.48	88.85	2.37

3.2. Textural properties and structural characterization of catalysts

The BET surface areas, pore volumes, and average pore sizes of the VMo/Ti, $VMoS_2$(H)/Ti, and $VMoS_2$(T)/Ti catalysts are listed in Table 1. Their specific surface area values are similar (77 m^2g^{-1}, 72 m^2g^{-1}, and 77 m^2g^{-1} for VMo/Ti, $VMoS_2$(H)/Ti, and $VMoS_2$(T)/Ti, respectively). The majority of the catalyst composition consists of TiO_2 support, thus, no discernible differences in specific surface area values were observed based on variations in the Mo precursor. The pore volume and average pore size values are all approximately the same for all catalysts. These results suggest that the BET surface area and porosity are not the key factors for the different catalytic activities [37].

The XRD patterns of the VMo/Ti, $VMoS_2$(H)/Ti, and $VMoS_2$(T)/Ti catalysts calcined at 500°C for 4 h are shown in Fig. 3a. All the characteristic diffraction peaks are related to tetragonal anatase TiO_2, and no other metal oxide peaks are observed [38]. The absence of V and Mo peaks in all the catalysts suggests the presence of highly dispersed amorphous metal oxides on the TiO_2 support [39], which confirms the successful synthesis of all the catalysts. Fig. 3b presents the Raman spectra of the catalysts. The E_g, B_{1g}, A_{1g}, and E_g modes are assigned to the bands at 145–149, 343, 515, and 638 cm^{-1}, respectively, corresponding to the characteristic bands of anatase TiO_2 [40,41]. To confirm the structure of VO_X, we reduced the TiO_2 content in the three catalysts and conducted additional Raman analysis, as illustrated in Fig. S1.

3.3. SCR catalytic activity test

Elemental compositions of the VMo/Ti, $VMoS_2$(H)/Ti, and $VMoS_2$(T)/Ti catalysts were determined using XRF, and the results are listed in Table 2. The catalyst contents were similar to the theoretically calculated values. Fig. 4 compares the NO_X conversion and N_2 selectivity of the catalysts synthesized using different Mo precursors, namely 1T/2H-MoS_2, 2H-MoS_2, and ammonium molybdate tetrahydrate. In the operating temperature range of 150-400°C with an interval of 50°C, all the catalysts, i.e., VMo/Ti, $VMoS_2$(H)/Ti, and $VMoS_2$(T)/Ti, show high NO_X conversion of 90.7, 96.3, and 99.7% at 350°C. Among them, the $VMoS_2$(T)/Ti catalyst demonstrates the highest NO_X conversion (96.5%) at 250°C. The NO_X conversion efficiencies using VMo/Ti and $VMoS_2$(H)/Ti catalysts are similar; however, the VMo/Ti catalyst has high efficiency at low temperatures, and $VMoS_2$(H)/Ti catalyst shows relatively high efficiency at high temperatures. Fig. 4b displays the N_2 selectivity over the same temperature range. All catalysts maintain 100% selectivity up to 300°C, but the selectivity of VMo/Ti significantly decreases after 350°C. In contrast, $VMoS_2$(H)/Ti and $VMoS_2$(T)/Ti catalysts maintain their N_2 selectivity up to 86.4 and 89.1%, respectively, even when the reaction temperature rises above 350°C.

The NH_3-SCR deactivation by SO_2 was evaluated for VMo/TiO_2 after the introduction of MoS_2 as the Mo precursor. Fig. 5 shows the NO_X conversion efficiencies using VMo/Ti, $VMoS_2$(H)/Ti, and $VMoS_2$(T)/Ti catalysts when 300 ppm SO_2 is introduced at 200°C. The NOx conversion of the $VMoS_2$(T)/Ti catalyst is 79% before and after the SO_2 injection. The VMo/Ti and $VMoS_2$/Ti(H) catalysts show NO_X conversion

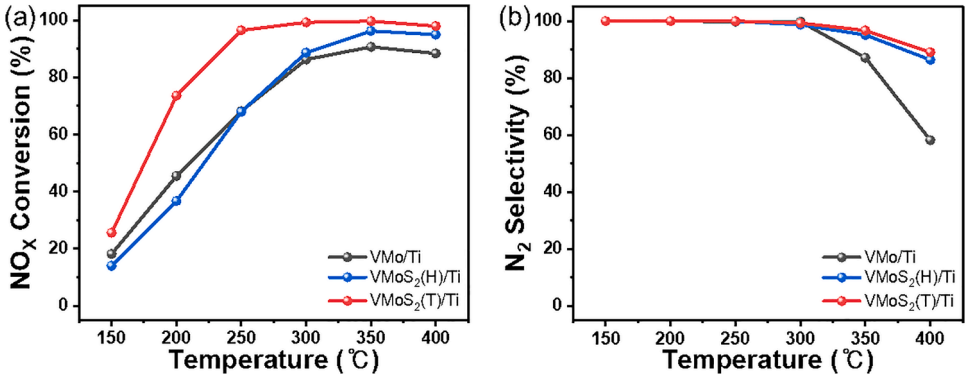

Fig. 4. (a) NO_X conversion and (b) N_2 selectivity of catalysts as a function of reaction temperature. (Reaction conditions: 300 ppm NO, 300 ppm NH_3, 5 vol% O_2, N_2 balanced gas, and GHSV 120,000 h^{-1}).

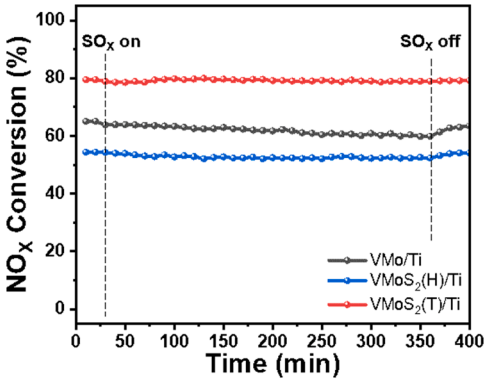

Fig. 5. SO_2-resistance in NH_3-SCR reaction at 200°C (Reaction conditions: 300 ppm NO, 300 ppm NH_3, 5 vol% O_2, 300 ppm SO_2, N_2 balanced gas, and GHSV 90,000 h^{-1}).

Table 3
The valence states of V, Mo, and O in the catalysts according to XPS results.

Catalysts	$V^{4+}/(V^{4+}+V^{5+})$	$Mo^{6+}/(Mo^{6+}+Mo^{5+})$	$O_{surface}/O_{total}$
VMo/Ti	46.7	26.4	50.3
$VMoS_2$(H)/Ti	33.1	32.7	64.8
$VMoS_2$(T)/Ti	56.3	34.7	62.5

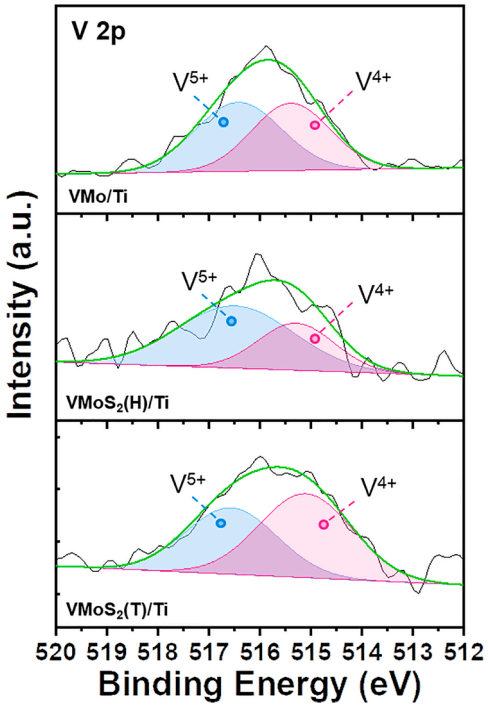

Fig. 6. XPS spectra of VMo/Ti, $VMoS_2$(H)/Ti, and $VMoS_2$(T)/Ti at the V 2p core level.

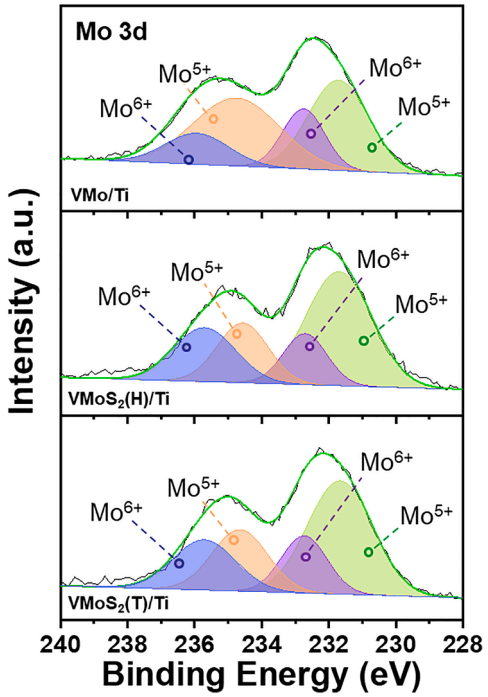

Fig. 7. XPS spectra of VMo/Ti, $VMoS_2$(H)/Ti, and $VMoS_2$(T)/Ti at the Mo 3d core level.

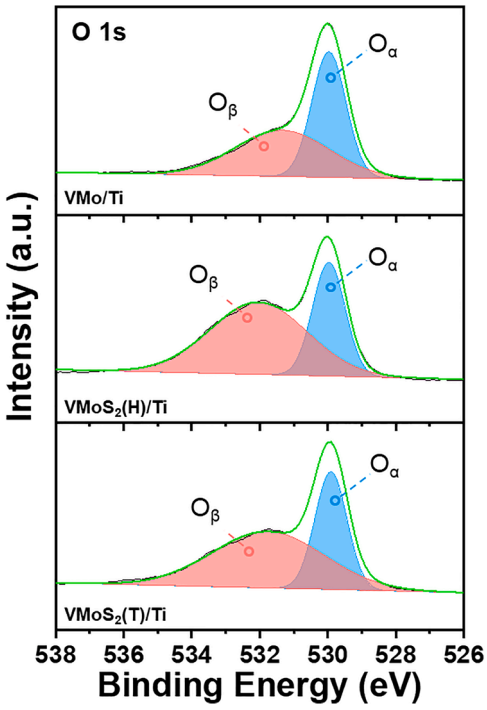

Fig. 8. XPS spectra of VMo/Ti, $VMoS_2$(H)/Ti, and $VMoS_2$(T)/Ti at the O 1s core level.

efficiencies of 60 and 53%, respectively, which is a 5 and 2% reduction from their initial efficiencies. Therefore, the $VMoS_2$(T)/Ti catalyst incorporated with 1T/2H-MoS_2 exhibits the best SCR catalytic performance and SO_2-resistance. However, when the initial efficiency is not considered, the catalyst using MoS_2 as the Mo precursor demonstrates enhanced SO_2-resistance regardless of the phase state. Further, XPS and FT-IR spectroscopy were used to analyze the synthesized catalysts and the oxidation degree introduced by 1T/2H-MoS_2. Particularly, the enhancement in SO_2-resistance was investigated by FT-IR by analyzing the materials generated on the catalyst surface after the SO_2-poisoning test. To further demonstrate the SO_2 resistance effect, SO_2-poisoning tests were performed on the three catalysts by introducing SO_2 under more harsh conditions at a lower temperature of 175°C (Fig. S2).

3.4. Surface chemical states of catalysts

The chemical states of various elements in the catalysts, such as V, Mo, and O, are important for determining the NH_3-SCR catalytic efficiency and SO_2-resistance enhancement as they affect the redox properties [42]. The surface states and atomic concentrations of all the catalysts were obtained via XPS and summarized in Table 3, and the XPS spectra at V 2p, Mo 3d, and O 1s core levels are displayed in Fig. 6–8. The V 2p peaks are deconvoluted to two valence states, i.e., V^{4+} (515.7–516.2 eV) and V^{5+} (516.4–517.0 eV) [43,44]. Table 3 summarizes the valence state ratios of different elements; in the case of vanadium, the $V^{4+}/(V^{4+}+V^{5+})$ values are 46.7%, 33.1%, and 56.3 % for VMo/Ti, $VMoS_2$(H)/Ti, and $VMoS_2$(T)/Ti, respectively. As shown in Fig. 4, the catalytic efficiency decreases in the order of $VMoS_2$(T)/Ti> VMo/Ti> $VMoS_2$(H)/Ti below 300°C, which is in accordance with the order of $V^{4+}/(V^{4+}+V^{5+})$. It is well-known that the oxidation state V^{4+} of the vanadium species is favorable for NO_X conversion [45]. The non-stoichiometric V^{4+} can enhance the NH_3-SCR catalytic performance because it has more electrons than the stable V^{5+} state [46,47].

Fig. 7 shows the Mo 3d spectra of all the catalysts. The Mo 3d peak is deconvoluted into two species, Mo^{5+} (231.7 and 234.9 eV) and Mo^{6+} (232.65 and 235.85 eV). The $Mo^{6+}/(Mo^{5+}+Mo^{6+})$ ratio on the surface is summarized in Table 3. As a catalytic promoter, molybdenum can resist

SO_2 poisoning, and the higher the Mo^{6+} ratio, the better the resistance to poisoning [28,48]. As shown in Fig. 4, $VMoS_2$(T)/Ti and $VMoS_2$(H)/Ti catalysts exhibit better SO_2 resistance than the VMo/Ti catalyst, which shows a rapid reduction in NO_X conversion rate owing to SO_2-poisoning. The ratios of Mo^{6+} to the total Mo for $VMoS_2$(T)/Ti and $VMoS_2$(H)/Ti catalysts are 34.7 and 32.7%, respectively, significantly higher than that of VMo/Ti (26.4%). The results imply that Mo^{6+} on the catalyst surface is advantageous for SO_2-resistance [29,49]. Therefore, regardless of the phase state, the $Mo^{6+}/(Mo^{5+}+Mo^{6+})$ ratio in the catalysts increases with the addition of MoS_2, and the $VMoS_2$(T)/Ti and $VMoS_2$(H)/Ti catalysts exhibit excellent SO_2 resistance. Particularly, the $VMoS_2$(T)/Ti catalyst incorporated with 1T/2H-MoS_2 displays a high NH_3-SCR activity due to its high $V^{4+}/(V^{4+}+V^{5+})$ ratio. Additionally, the more Mo^{6+} in this catalyst corresponds to its better SO_2-resistance.

Fig. 8 shows the O 1s spectra of the VMo/Ti, $VMoS_2$(H)/Ti, and $VMoS_2$(T)/Ti catalysts. The O 1s peaks can be fitted into lattice oxygen (O_α) and surface-adsorbed oxygen (O_β) [50]. Their binding energies were measured at 529.4–530.4 eV for lattice oxygen and 530.1–532.0 eV for surface adsorbed oxygen [51]. The O_β ratio was calculated using $O_{surface}/O_{total}$, and a higher amount of O_β in the catalysts can promote oxygen diffusion and increase oxygen mobility [52,53]. Similar to the observation in Fig. 7, the catalysts prepared using MoS_2 precursor demonstrate high surface adsorbed oxygen ratios. Specifically, $VMoS_2$(H)/Ti, $VMoS_2$(T)/Ti, and VMo/Ti catalysts exhibit oxygen ratios of 64.8, 62.5, and 50.3% respectively (Table 3). According to the results in Fig. 6 and Table 3, the $VMoS_2$(H)/Ti catalyst with the smallest $V^{4+}/(V^{4+}+V^{5+})$ ratio shows a similar NO_X conversion to that of the VMo/Ti catalyst because it has the highest $O_{surface}/O_{total}$ ratio. The result suggests that a high surface adsorbed oxygen ratio enhances the redox capacity of the NH_3-SCR reaction [54,55].

3.5. Formation of sulfate species on the catalysts

To identify the factors responsible for improving the SO_2-resistance, FT-IR spectra of the catalyst incorporated with 1T/2H-MoS_2 before and after the SO_2-resistance test were obtained, and the functional groups on the surface were studied. As shown in Fig. 9 a and b, the bands at 1224 and 1043 cm^{-1} are assigned to bidentate SO_4^{-2} and the symmetric stretching vibrations of sulfonates (SO_3^-), respectively [56,57]. These bands appear only in the MoS_2-incorporated catalysts and are referred to as S-related bands formed by the S in MoS_2. However, after SO_2-poisoning, new bands appear at 1625, 1445, 1419, 1384, 1132, 1120, 1067, and 1035 cm^{-1}. The band of 1625 cm^{-1} is assigned to the O-H bending mode, which corresponds to the physically absorbed water. The 1445–1430 cm^{-1} bands can arise from the ammonium ions formed during the NH_3-SCR reaction. The band at 1419 cm^{-1} is assigned to the NH_4^+ adsorbed on the Brønsted acid site, indicating that the NH_4^+ species are generated after SO_2 poisoning owing to the deposition of ammonium sulfates such as $(NH_4)_2SO_4$ and NH_4HSO_4 [58,59]. This peak appears only in the SO_2-poisoned VMo/Ti catalyst, implying that the decrease in NO_X conversion is due to the formation of ammonium sulfates on the surface. The band at 1384 cm^{-1} indicates the presence of surface sulfate species with covalently bonded S=O configurations. This signifies the formation of triply bridged sulfate on the surface [60]. The band at 1132 cm^{-1} involves the contributions of –OH stretching vibration. The band at approximately 1120 cm^{-1} is due to the formation of $(NH_4)_2SO_4$ by surface sulfate and ammonia species adsorption [58,61]. The bands at approximately 1110 cm^{-1} are related to the S-O symmetric and asymmetric stretching modes of SO_4^{2-} [62]. The VMo/Ti catalyst shows a stronger SO_2 band than the other catalysts, confirming its vulnerability to SO_2 poisoning. Therefore, its NO_X conversion performance tends to degrade during the SO_2-resistance test. The improved SO_2 resistance in the other two catalysts with added MoS_2 can be confirmed by the minor intensity change in the peak owing to the S of MoS_2.

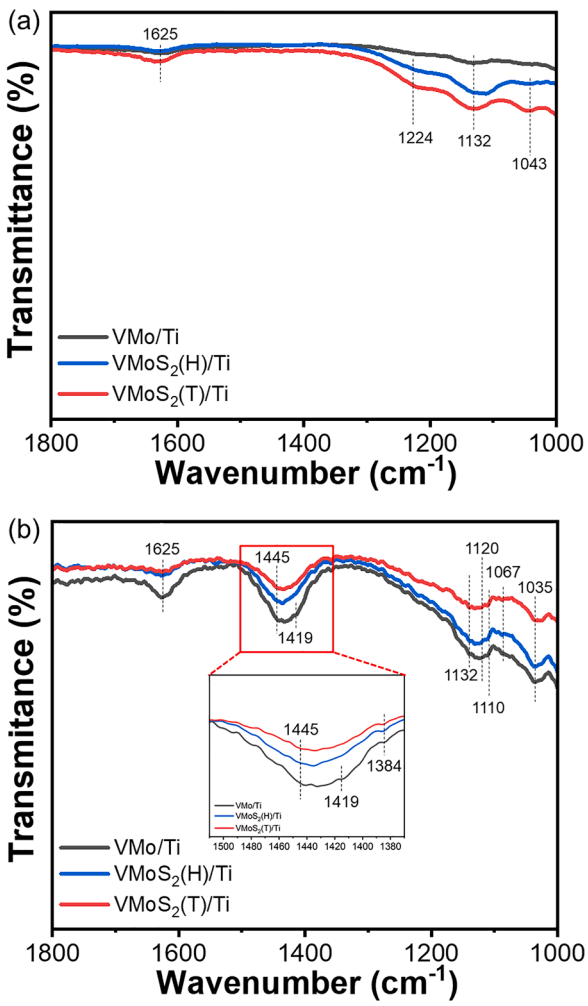

Fig. 9. (a) FT-IR spectra of fresh VMo/Ti, $VMoS_2$(H)/Ti, and $VMoS_2$(T)/Ti catalysts. (b) FT-IR spectra of VMo/Ti, $VMoS_2$(H)/Ti, and $VMoS_2$(T)/Ti catalysts after the SO_2-resistance test.

4. Conclusion

In this study, the effects of using 1T/2H-MoS_2 as a precursor to prepare vanadium-based catalysts on temperature sensitivity and SO_2-resistance were tested. Ammonium molybdate tetrahydrate was replaced with 2H-MoS_2 and heterogeneous 1T/2H-MoS_2 as molybdenum precursors for the VMo/TiO_2 catalysts. The NO_X conversion efficiency of the vanadium-based catalyst was affected by the valence state ratios of $V^{4+}/(V^{4+}+V^{5+})$ and $O_{surface}/O_{total}$. The SO_2 resistance was improved when MoS_2 was incorporated regardless of the phase state because of the increased amount of Mo^{6+} in the catalysts. In addition, the surface functional groups in the SO_2-poisoned and fresh catalysts were evaluated by FT-IR. The VMo/Ti was vulnerable to SO_2 poisoning because the surface acid site was degraded. Ultimately, a catalyst with high SCR activity over a wide temperature range (250 to 400°C) and SO_2 resistance was synthesized by utilizing the heterogeneous 1T/2H-MoS_2 precursor.

CRediT authorship contribution statement

Su-Jin Kim: Writing – original draft, Investigation, Conceptualization, Validation. **Donghyeok Kim:** Formal analysis, Visualization. **Myeung-Jin Lee:** Writing – review & editing. **Woon-Gi Kim:** Investigation, Software. **Bora Jeong:** Data curation. **Bora Ye:** Supervision,

Conceptualization, Writing – review & editing. **Hong-Dae Kim:** Supervision, Conceptualization.

Declaration of competing interest

The authors declare that they have no known competing financial interests or personal relationships that could have appeared to influence the work reported in this paper.

Data availability

No data was used for the research described in the article.

Acknowledgements

This research was financially supported by the Ministry of Trade, Industry and Energy (MOTIE) (No. 20015619) and the National Research Foundation of Korea (NRF) grant funded by the Korea government (MSIT) (No. RS-2023-00282392). We would like to express our sincere thanks to their support.

Supplementary materials

Supplementary material associated with this article can be found, in the online version, at doi:10.1016/j.surfin.2023.103780.

References

[1] J. Liu, R.-t. Guo, M.-y. Li, P. Sun, S.-m. Liu, W.-g. Pan, S.-w. Liu, X. Sun, Enhancement of the SO_2 resistance of Mn/TiO_2 SCR catalyst by Eu modification: A mechanism study, Fuel 223 (2018) 385–393, https://doi.org/10.1016/j.fuel.2018.03.062.

[2] Q. Li, X. Hou, H. Yang, Z. Ma, J. Zheng, F. Liu, X. Zhang, Z. Yuan, Promotional effect of CeO_X for NO reduction over V_2O_5/TiO_2-carbon nanotube composites, Journal of Molecular Catalysis A: Chemical 356 (2012) 121–127, https://doi.org/10.1016/j.molcata.2012.01.004.

[3] Y.Q. Zhu, W.H. Zhou, C. Xia, Q.C. Hou, Application and Development of Selective Catalytic Reduction Technology for Marine Low-Speed Diesel Engine: Trade-Off among High Sulfur Fuel, High Thermal Efficiency, and Low Pollution Emission, ATMOSPHERE 13 (2022), https://doi.org/10.3390/atmos13050731.

[4] S. Luo, W. Zhou, A. Xie, F. Wu, C. Yao, X. Li, S. Zuo, T. Liu, Effect of MnO2 polymorphs structure on the selective catalytic reduction of NOx with NH_3 over TiO_2–Palygorskite, Chemical Engineering Journal 286 (2016) 291–299, https://doi.org/10.1016/j.cej.2015.10.079.

[5] W. Tian, H. Yang, X. Fan, X. Zhang, Catalytic reduction of NOx with NH_3 over different-shaped MnO_2 at low temperature, Journal of Hazardous Materials 188 (2011) 105–109, https://doi.org/10.1016/j.jhazmat.2011.01.078.

[6] C.P. Cho, Y.D. Pyo, J.Y. Jang, G.C. Kim, Y.J. Shin, NOx reduction and N_2O emissions in a diesel engine exhaust using Fe-zeolite and vanadium based SCR catalysts, Applied Thermal Engineering 110 (2017) 18–24, https://doi.org/10.1016/j.applthermaleng.2016.08.118.

[7] X. Huang, D. Wang, H. Zhao, Q. Yang, Y. Peng, J. Li, Severe deactivation and artificial enrichment of thallium on commercial SCR catalysts installed in cement kiln, Applied Catalysis B: Environmental 277 (2020) 119194, https://doi.org/10.1016/j.apcatb.2020.119194.

[8] P.C. Hung, S.H. Chang, S.H. Lin, A. Buekens, M.B. Chang, Pilot Tests on the Catalytic Filtration of Dioxins, Environmental Science & Technology 48 (2014) 3995–4001, https://doi.org/10.1021/es404926g.

[9] X. Du, X. Gao, K. Qiu, Z. Luo, K. Cen, The Reaction of Poisonous Alkali Oxides with Vanadia SCR Catalyst and the Afterward Influence: A DFT and Experimental Study, The Journal of Physical Chemistry C 119 (2015) 1905–1912, https://doi.org/10.1021/jp511475b.

[10] J. Huang, J. Chen, J. Yao, S. Zhao, X. Wu, Q. Xia, Novel regenerated V- and Ce-mixed oxide modified catalysts for the NH_3-SCR of NOx displaying a distinctive broad temperature window, Journal of Cleaner Production 382 (2023) 135384, https://doi.org/10.1016/j.jclepro.2022.135384.

[11] Y. He, M.E. Ford, M. Zhu, Q. Liu, U. Tumuluri, Z. Wu, I.E. Wachs, Influence of catalyst synthesis method on selective catalytic reduction (SCR) of NO by NH_3 with V_2O_5-WO_3/TiO_2 catalysts, Applied Catalysis B: Environmental 193 (2016) 141–150, https://doi.org/10.1016/j.apcatb.2016.04.022.

[12] Z. Shi, Q. Peng, J. E, B. Xie, J. Wei, R. Yin, G. Fu, Mechanism, performance and modification methods for NH_3-SCR catalysts: A review, Fuel 331 (2023) 125885, https://doi.org/10.1016/j.fuel.2022.125885.

[13] L. Jiang, Q. Liu, G. Ran, M. Kong, S. Ren, J. Yang, J. Li, V_2O_5-modified Mn-Ce/AC catalyst with high SO_2 tolerance for low-temperature NH_3-SCR of NO, Chemical Engineering Journal 370 (2019) 810–821, https://doi.org/10.1016/j.cej.2019.03.225.

[14] D. Damma, P.R. Ettireddy, B.M. Reddy, P.G. Smirniotis, A Review of Low Temperature NH_3-SCR for Removal of NOx, CATALYSTS 9 (2019), https://doi.org/10.3390/catal9040349.

[15] G. Xu, H. Wang, Y. Yu, H. He, Role of silver species in H_2-NH_3-SCR of NOx over Ag/Al_2O_3 catalysts: Operando spectroscopy and DFT calculations, Journal of Catalysis 395 (2021) 1–9, https://doi.org/10.1016/j.jcat.2020.12.025.

[16] B. Ye, B. Jeong, M.J. Lee, T.H. Kim, S.S. Park, J. Jung, S. Lee, H.D. Kim, Recent trends in vanadium-based SCR catalysts for NOx reduction in industrial applications: stationary sources, NANO CONVERGENCE 9 (2022), https://doi.org/10.1186/s40580-022-00341-7.

[17] J. Arfaoui, A. Ghorbel, C. Petitto, G. Delahay, Novel V_2O_5-CeO_2-TiO_2-SO_4^{2-} nanostructured aerogel catalyst for the low temperature selective catalytic reduction of NO by NH_3 in excess O_2, Applied Catalysis B: Environmental 224 (2018) 264–275, https://doi.org/10.1016/j.apcatb.2017.10.059.

[18] M. Zhang, B. Huang, H. Jiang, Y. Chen, Research progress in the SO_2 resistance of the catalysts for selective catalytic reduction of NOx, Chinese Journal of Chemical Engineering 25 (2017) 1695–1705, https://doi.org/10.1016/j.cjche.2017.03.030.

[19] J. Sun, X.J. Li, W.L. Guo, M. Zhao, X. Fan, Y.B. Dong, C. Xu, J. Deng, Y.F. Fu, Synthesis Methods of Two-Dimensional MoS_2: A Brief Review, CRYSTALS 7 (2017), https://doi.org/10.3390/cryst7070198.

[20] J. Mao, Y. Wang, Z.L. Zheng, D.H. Deng, The rise of two-dimensional MoS_2 for catalysis, FRONTIERS OF PHYSICS 13 (2018), https://doi.org/10.1007/s11467-018-0812-0.

[21] Y. Linghu, T. Tong, C. Li, C. Wu, The catalytic mechanism of CO_2 electrochemical reduction over transition metal-modified 1T'-MoS_2 monolayers, Applied Surface Science 590 (2022) 153001, https://doi.org/10.1016/j.apsusc.2022.153001.

[22] X. Li, K. Peng, Hydrothermal synthesis of MoS_2 nanosheet/palygorskite nanofiber hybrid nanostructures for enhanced catalytic activity, Applied Clay Science 162 (2018) 175–181, https://doi.org/10.1016/j.clay.2018.06.015.

[23] H.W. Xu, J.W. Zhu, Q.L. Ma, J.J. Ma, H.W. Bai, L. Chen, S.C. Mu, Two-Dimensional MoS_2: Structural Properties, Synthesis Methods, and Regulation Strategies toward Oxygen Reduction, MICROMACHINES 12 (2021), https://doi.org/10.3390/mi12030240.

[24] S. K, A. J, H. S, N. M, S. GR, P. S, M. C, H. K, One-step fabrication of ultrathin layered 1T@2H phase MoS_2 with high catalytic activity based counter electrode for photovoltaic devices, Journal of Materials Science & Technology 51 (2020) 94–101, https://doi.org/10.1016/j.jmst.2020.01.024.

[25] Z. Liu, Z. Gao, Y. Liu, M. Xia, R. Wang, N. Li, Heterogeneous Nanostructure Based on 1T-Phase MoS_2 for Enhanced Electrocatalytic Hydrogen Evolution, ACS Applied Materials & Interfaces 9 (2017) 25291–25297, https://doi.org/10.1021/acsami.7b05775.

[26] X. Ren, L. Pang, Y. Zhang, X. Ren, H. Fan, S. Liu, One-step hydrothermal synthesis of monolayer MoS_2 quantum dots for highly efficient electrocatalytic hydrogen evolution, Journal of Materials Chemistry A 3 (2015) 10693–10697, https://doi.org/10.1039/C5TA02198G.

[27] Y.X. Yao, K.L. Ao, P.F. Lv, Q.F. Wei, MoS(2)Coexisting in 1T and 2H Phases Synthesized by Common Hydrothermal Method for Hydrogen Evolution Reaction, NANOMATERIALS 9 (2019), https://doi.org/10.3390/nano9060844.

[28] D.W. Kwon, K.H. Park, S.C. Hong, Enhancement of SCR activity and SO_2 resistance on VOx/TiO_2 catalyst by addition of molybdenum, Chemical Engineering Journal 284 (2016) 315–324, https://doi.org/10.1016/j.cej.2015.08.152.

[29] D.W. Kwon, K.H. Park, H.P. Ha, S.C. Hong, The role of molybdenum on the enhanced performance and SO_2 resistance of V/Mo-Ti catalysts for NH_3-SCR, Applied Surface Science 481 (2019) 1167–1177, https://doi.org/10.1016/j.apsusc.2019.03.118.

[30] H.G. Im, M.J. Lee, W.G. Kim, S.J. Kim, B. Jeong, B. Ye, H. Lee, H.D. Kim, High-Dispersed V_2O_5-CuOX Nanoparticles on h-BN in NH_3-SCR and NH_3-SCO Performance, NANOMATERIALS 12 (2022), https://doi.org/10.3390/nano12142329.

[31] J. Gu Heo, M. Ullah, M.-P. Chun, Y. Sik Chu, S. Gwan Seo, M. Chae Seo, Y. Son Choe, D.-S. Kim, Low-temperature shift DeNOx activity of Nanoflake V_2O_5 loaded WO_3/TiO_2 as NH_3-SCR catalyst, Inorganic Chemistry Communications 137 (2022) 109191, https://doi.org/10.1016/j.inoche.2021.109191.

[32] X.L. Li, T.C. Li, S. Huang, J. Zhang, M.E. Pam, H.Y. Yang, Controllable Synthesis of Two-Dimensional Molybdenum Disulfide (MoS_2) for Energy-Storage Applications, ChemSusChem 13 (2020) 1379–1391, https://doi.org/10.1002/cssc.201902706.

[33] D. Saha, P. Kruse, Editors' Choice—Review—Conductive Forms of MoS_2 and Their Applications in Energy Storage and Conversion, Journal of The Electrochemical Society 167 (2020) 126517, https://doi.org/10.1149/1945-7111/abb34b.

[34] H.L. Wei, A.D. Tan, W.B. Liu, J.H. Piao, K. Wan, Z.X. Liang, Z.P. Xiang, Z.Y. Fu, Interface Engineering-Induced 1T-MoS_2/NiS Heterostructure for Efficient Hydrogen Evolution Reaction, CATALYSTS 12 (2022), https://doi.org/10.3390/catal12090947.

[35] Z. Xia, Y. Tao, Z. Pan, X. Shen, Enhanced photocatalytic performance and stability of 1T MoS_2 transformed from 2H MoS_2 via Li intercalation, Results in Physics 12 (2019) 2218–2224, https://doi.org/10.1016/j.rinp.2019.01.020.

[36] U. Gupta, B.S. Naidu, U. Maitra, A. Singh, S.N. Shirodkar, U.V. Waghmare, C.N. R. Rao, Characterization of few-layer 1T-$MoSe_2$ and its superior performance in the visible-light induced hydrogen evolution reaction, APL Materials 2 (2014) 092802, https://doi.org/10.1063/1.4892976.

[37] H. Wang, B. Wang, J. Zhou, G. Li, D. Zhang, Z. Ma, R. Xiong, Q. Sun, W.Q. Xu, CuO modified vanadium-based SCR catalysts for Hg^0 oxidation and NO reduction, Journal of Environmental Management 239 (2019) 17–22, https://doi.org/10.1016/j.jenvman.2019.02.118.

[38] Z. Xuteng, A relationship between the V^{4+}/V^{5+} ratio and the surface dispersion, surface acidity, and redox performance of V_2O_5–WO_3/TiO_2 SCR catalysts, RSC advances 8 (2018) 31081–31093, https://doi.org/10.1039/c8ra02857e, v.2018 v.8 no.54.
[39] Z. Liu, S. Zhang, J. Li, L. Ma, Promoting effect of MoO_3 on the NOx reduction by NH_3 over CeO_2/TiO_2 catalyst studied with in situ DRIFTS, Applied Catalysis B: Environmental 144 (2014) 90–95, https://doi.org/10.1016/j.apcatb.2013.06.036.
[40] L. Chu, Z.F. Qin, J.P. Yang, X.A. Li, Anatase TiO_2 Nanoparticles with Exposed {001} Facets for Efficient Dye-Sensitized Solar Cells, SCIENTIFIC REPORTS 5 (2015), https://doi.org/10.1038/srep12143.
[41] S.S. El-Deen, A.M. Hashem, A.E.A. Ghany, S. Indris, H. Ehrenberg, A. Mauger, C. M. Julien, Anatase TiO_2 nanoparticles for lithium-ion batteries, IONICS 24 (2018) 2925–2934, https://doi.org/10.1007/s11581-017-2425-y.
[42] J. Kim, J. Min Won, S. Kwan Jeong, K. Yu, K. Shin, S.-M. Hwang, Fe-promoted V/W/TiO_2 catalysts for enhanced low-temperature denitrification efficiency, Applied Surface Science 601 (2022) 154290, https://doi.org/10.1016/j.apsusc.2022.154290.
[43] A. Shi, X. Wang, T. Yu, M. Shen, The effect of zirconia additive on the activity and structure stability of V_2O_5/WO_3-TiO_2 ammonia SCR catalysts, Applied Catalysis B: Environmental 106 (2011) 359–369, https://doi.org/10.1016/j.apcatb.2011.05.040.
[44] F. Han, Y.C. Gao, Q.H. Huo, L.N. Han, J.C. Wang, W.R. Bao, L.P. Chang, Characteristics of Vanadium-Based Coal Gasification Slag and the NH_3-Selective Catalytic Reduction of NO, CATALYSTS 8 (2018), https://doi.org/10.3390/catal8080327.
[45] C.P. Qi, W.J. Bao, L.G. Wang, H.Q. Li, W.F. Wu, Study of the V_2O_5-WO_3/TiO_2 Catalyst Synthesized from Waste Catalyst on Selective Catalytic Reduction of NOx by NH_3, CATALYSTS 7 (2017), https://doi.org/10.3390/catal7040110.
[46] G.-j. Dong, Y. Bai, Y.-f. Zhang, Y. Zhao, Effect of the $V^{4+(3+)}/V^{5+}$ ratio on the denitration activity for V_2O_5–WO_3/TiO_2 catalysts, New Journal of Chemistry 39 (2015) 3588–3596, https://doi.org/10.1039/C5NJ00015G.
[47] P.-W. Seo, J.-Y. Lee, K.-S. Shim, S.-H. Hong, S.-C. Hong, S.-I. Hong, The control of valence state: How V/TiO_2 catalyst is hindering the deactivation using the mechanochemical method, Journal of Hazardous Materials 165 (2009) 39–47, https://doi.org/10.1016/j.jhazmat.2008.09.119.
[48] H. Al-Kandari, F. Al-Kharafi, N. Al-Awadi, O.M. El-Dusouqui, S.A. Ali, A. Katrib, The catalytic active sites in partially reduced MoO_3 for the hydroisomerization of 1-pentene and n-pentane, Applied Catalysis A: General 295 (2005) 1–10, https://doi.org/10.1016/j.apcata.2005.07.023.
[49] Z. Chen, X. Wu, K. Ni, H. Shen, Z. Huang, Z. Zhou, G. Jing, Molybdenum-decorated V_2O_5–WO_3/TiO_2: surface engineering toward boosting the acid cycle and redox cycle of NH_3-SCR, Catalysis Science & Technology 11 (2021) 1746–1757, https://doi.org/10.1039/D0CY02147D.
[50] Z. Yaping, Improved activity of Ho-modified Mn/Ti catalysts for the selective catalytic reduction of NO with NH_3, Environmental science and pollution research 27 (2020) 26954–26964, https://doi.org/10.1007/s11356-020-07749-w, v.2020 v.27 no.21.
[51] L. Lu, X.M. Wang, C.H. Hu, Y. Liu, X.B. Chen, P. Fang, D.S. Chen, C.P. Cen, ISNanosized V-Ce Oxides Supported on TiO_2 as a Superior Catalyst for the Selective Catalytic Reduction of NO, CATALYSTS 10 (2020), https://doi.org/10.3390/catal10020202.
[52] S. Zhang, Q. Zhang, Y. Zhao, J. Yang, Y. Xu, J. Zhang, Enhancement of CeO_2 modified commercial SCR catalyst for synergistic mercury removal from coal combustion flue gas, RSC Advances 10 (2020) 25325–25338, https://doi.org/10.1039/D0RA04350H.
[53] G. Cui, X. Zhang, H. Wang, Z. Li, W. Wang, Q. Yu, L. Zheng, Y. Wang, J. Zhu, M. Wei, ZrO_2-x modified Cu nanocatalysts with synergistic catalysis towards carbon-oxygen bond hydrogenation, Applied Catalysis B: Environmental 280 (2021) 119406, https://doi.org/10.1016/j.apcatb.2020.119406.
[54] S. Raja, M.S. Alphin, Systematic effects of Fe doping on the activity of V_2O_5/TiO_2-carbon nanotube catalyst for NH_3-SCR of NOx, JOURNAL OF NANOPARTICLE RESEARCH 22 (2020), https://doi.org/10.1007/s11051-020-04919-2.
[55] X. Wu, J. Liu, X. Liu, X. Wu, Y. Du, Fabrication of carbon doped Cu-based oxides as superior NH_3-SCR catalysts via employing sodium dodecyl sulfonate intercalating CuMgAl-LDH, Journal of Catalysis 407 (2022) 265–280, https://doi.org/10.1016/j.jcat.2022.02.004.
[56] L.Y. Wang, P. Gui, Y. Shen, C.R. Gong, G. Xue, Effect of Tourmaline Addition on the Catalytic Performance and SO_2 Resistance of $NixMn_3$-xO_4 Catalyst for NH_3-SCR Reaction at Low Temperature, CATALYSIS LETTERS 151 (2021) 3404–3416, https://doi.org/10.1007/s10562-021-03585-w.
[57] X. Wenqing, Effects of MoO_3 and CeO_2 doping on the decomposition and reactivity of NH_4HSO_4 on V_2O_5/TiO_2 catalysts, Environmental science and pollution research international 27 (2020) 30243–30253, https://doi.org/10.1007/s11356-020-09343-6, v2020 v.27 no.24.
[58] Z. Bolin, Selective catalytic reduction of NOx with NH_3 over Mn–Zr–Ti mixed oxide catalysts, Journal of materials science. v. 54 (2019) 6943–6960, https://doi.org/10.1007/s10853-019-03369-z, 2019 v.54 no.9.
[59] J. Yu, F. Guo, Y. Wang, J. Zhu, Y. Liu, F. Su, S. Gao, G. Xu, Sulfur poisoning resistant mesoporous Mn-base catalyst for low-temperature SCR of NO with NH_3, Applied Catalysis B: Environmental 95 (2010) 160–168, https://doi.org/10.1016/j.apcatb.2009.12.023.
[60] H.A. Khalaf, S.E. Mansour, E.A. El-Madani, The influence of sulfate contents on the surface properties of sulfate-modified tin(IV) oxide catalysts, Journal of the Association of Arab Universities for Basic and Applied Sciences 10 (2011) 15–20, https://doi.org/10.1016/j.jaubas.2011.06.003.
[61] F. Lin, Y. He, Z. Wang, Q. Ma, R. Whiddon, Y. Zhu, J. Liu, Catalytic oxidation of NO by O_2 over CeO_2–MnOx: SO_2 poisoning mechanism, RSC Advances 6 (2016) 31422–31430, https://doi.org/10.1039/C6RA03818B.
[62] X. Ma, R. Yang, R. Doig, A. Liu, M.A. Rankin, L.M. Croll, P. Zhang, J.R. Dahn, MnO_2/Fe_2O_3 Nanocomposite Sorbent for Gas Capture, ACS Applied Nano Materials (1) (2018) 6674–6682, https://doi.org/10.1021/acsanm.8b01457.